Electron states associated with 90° partial dislocations in germanium

Wang Yong-liang*
Department of Physics and Measurement Technology, Linköping University, S-581 83 Linköping, Sweden
(Received 24 January 1989)

The unreconstructed 90° partial dislocations in germanium are examined by means of a linear combination of atomic orbitals electron Hamiltonian with ten Gaussian-type atomic orbitals for every atom, which for a perfect crystal yields accurate results for both the valence- and conduction-band states. A pair of alternate unreconstructed 90° partial dislocations with corresponding stacking faults are incorporated via a supercell containing 256 atoms. When the bound electron states were evaluated, the translation symmetry both along the dislocation line and in the plane perpendicular to the dislocation line was exploited. A powerful mathematical approach for large sparse matrices makes it possible to treat this supercell, its size being large enough to decouple the interactions between neighboring dislocations. The deep energy levels in the gap and the resonant states were extracted with use of the Lanczos algorithm and a continued-fraction representation of the local density of states. Two defect bands for the 90° partial dislocation in germanium were obtained. In the center of the one-dimensional Brillouin zone the two bands are widely split and are joined together at the zone boundary. The upper band is a resonant state near the center of the zone and becomes a bound state at the zone boundary. The lower band is a bound state over the entire zone.

I. INTRODUCTION

Many of the most important properties of semiconductor materials and semiconductor devices are determined by the presence of lattice defects: point defects and dislocations. Dislocations in semiconductors seem at a first glance to be less important, since first they may well be avoided in growing single crystals and secondly they cannot move at room temperature. For a rather long time, dislocations in semiconductors were investigated in only a few places. The situation was somewhat changed when it became known that dislocations may be produced not only during device fabrication, but also afterwards in devices working at elevated temperature. Well-known examples are dislocations which make semiconductor lasers deteriorate and shorten the lifetime of the devices. Recent years have seen an expansion in both the theoretical[1–3] and experimental[4] investigation of the deep electron levels associated with dislocations in plastically deformed covalent crystals.

Investigations using the weak-beam technique of electron microscopy show that the dislocation in silicon and germanium of either screw type or 60° type are dissociated into partial dislocations.[5–7] For the 60° dislocation a 30° partial dislocation and a 90° partial dislocation are formed through dissociation, while the screw splits into two 30° partial dislocations. Each of the dislocations has a total Burgers vector of the $\frac{1}{2}a(1,1,0)$ type lying on a $\{111\}$ slip plane with line direction $\langle 110\rangle$. Dislocations running in other directions in the lattice are to be thought of as kinked segments of these types. Thus, it is generally believed that the important elemental defects (other than point defects) which control the mechanical and electronic properties of tetrahedrally coordinated semiconductors at low temperatures are the 30° partial dislocation, the 90° partial dislocation, and kinks. These dislocation may also lie on either the closely spaced (111) glide planes or on the more widely spaced (111) "shuffle" planes.[8] Recent evidence[9] favors the glide model. The stacking faults associated with the partial dislocations are found to be either intrinsic or extrinsic, but a majority of intrinsic faults were reported.

It was generally accepted that there are no deep levels associated with the stacking faults,[10] whereas the dangling bonds in the core region of the dislocations have a great influence on the defect bands which can be resonant states or bound states. The exact structure of configurations in the core region of the dislocations is not clear at present either experimentally or theoretically. The lattice-model simulations for the core structure of the dislocations show that the partial dislocations may exist in different core configurations which, although being translationally invariant parallel to the dislocation line, differ with regard to the point symmetry of the atomic arrangements. It seems that the low-symmetric reconstructed cores of partial dislocations without dangling bonds are energetically more probable than the high-symmetric unreconstructed partial dislocations with dangling bonds in the core.

In investigating the deep levels of dislocations, the main technical problem arises from the fact that dislocations are topological defects of the lattice. The topological disorder introduced by a dislocation prevents one from modeling dislocations in a simple way by local perturbation potentials. The theoretical approachs developed for point-defect problems such as the Green-function method cannot be applied to the case of dislocations. Thus in all presently used methods the deep electron levels of dislocations are found by comparing calculated energy spectra of the crystals containing dislocations with those of perfect crystals.

Dislocations are one-dimensional defects, maintaining the translational symmetry of the lattice parallel to the dislocation line but destroying this symmetry in the plane

orthogonal to the dislocation line. However, in all the theoretical investigations made so far of the deep electron levels at dislocations in semiconductors, this symmetry is artificially modified by two methods. In the first method[11,12] the translational symmetry perpendicular to the dislocation line is restored by considering periodic arrangements of pairs of alternate dislocations forming a superlattice with large unit cells. In the second method,[13,14] the translational symmetry is ignored altogether. The crystal with a dislocation is modeled as a spherical cluster of a limited number of atoms (typically 700 to 1500) around a dislocation core, and the deep levels are determined from a continued-fraction density of states (DOS).[15]

In the spherical-cluster treatment of the deep electron levels at dislocations in Si, Jones[13] and Jones and Marklund[14] characterize the electron in the tight-binding interpolation scheme of Slater and Koster.[16] The parametrization developed by Pandey and Phillips[17] is used, with exponential scaling of the tight-binding parameters under deformations. In the supercell approach other treatment of electrons have been used. For example, for Si Northrup *et al.*[18] and Chelikowsky[19] used a Gaussian-orbital description combined with local-atomic-model potentials. They applied a standard technique of the band-structure calculation to the supercell. In order to reduce the size of the matrix while still retaining some of the variational content of the *d*-symmetry orbitals, they employ Louie's method of phase-dependent chemical orbitals.[20] Louie has shown that by properly preparing the *s*, *p*, and *d* orbitals, one may treat the *d* orbitals in a modified form of Löwdin's perturbation theory. In this method, the variational content of the *d* orbitals is included implicitly in an effective Hamiltonian whose dimension is determined by the number of *s* and *p* orbitals. This procedure reduces the dimension of the matrix by a factor 2.

For computational reasons the supercell method is applicable only to systems with small numbers of inequivalent atoms in a cell (typically about 56 to 88 atoms), which restricts consideration to narrow pairs of dislocations (hence interactions between localized states at different dislocations cannot be excluded) and rather simple dislocation-core structure. The spherical-cluster approach cannot resolve the dispersion of the deep level bands along the dislocation line since it artificially breaks the translational symmetry along the dislocations. Moreover, it has a rather limited energy resolution.

In the present paper by using a new mathematic approach for a large sparse matrix a supercell containing 256 atoms with a pair of alternate unreconstructed 90° partial dislocations and corresponding stacking faults were investigated for germanium. Because of the size of the supercell the interactions between localized states at different dislocations can be excluded and the translational symmetry both along the dislocation line and in the planes perpendicular to the dislocation can be exploited. Louie's Gaussian-type linear combination of atomic orbitals (LCAO) were employed, but the *d*-orbital content was included without recourse to the Löwdin perturbation theory. Recently this approach was applied to the 90° partial dislocations in Si.[21]

This paper is organized as follows. In Sec. II we will describe the approach we employed in forming the geometry of the supercell containing two alternate 90° partial dislocations and the method for calculating Hamilton matrix elements and overlap matrix elements between the rows of atoms along the direction of the dislocation line. The method on how to exploit the translation symmetry along the dislocation line and in the plane perpendicular to the dislocation line is also discussed. In the calculation of recursion coefficients we especially emphasize the problem of how to deal with the large nonorthogonal and sparse overlap matrix. In Sec. III, we present and discuss the results we obtained and make a comparison with the previous calculations and experiments.

II. CALCULATIONAL PROCEDURE

A. Formation of the supercell

The structures of dislocation cores are at present more or less unclear both experimentally and theoretically. The atomic coordinates for the dislocation structures can be taken from near-atomic–resolution-computed electron micrographs. Because the resolution of electron micrographs is at best 2 Å and the images sensitively depend on the electron optical parameters and specimen thickness, it is necessary afterwards to carry out an optimization procedure to reduce the bond-length and bond-angle deviations. Theoretically the core structures of dislocations are generated via lattice-model computer simulations proposed by Marklund.[10] Marklund used the valence-force-field potential of Keating[22] to determine atomic coordinates for both the 30° and 90° partial dislocations.

The simplest valence-force-field potential suggested by Keating is the one which expresses the elastic energy of an atom in the lattice according to the formula

$$E_K^H=\frac{3\alpha}{16r_0^2}\sum_{i=1}^{4}(\mathbf{r}_i\cdot\mathbf{r}_i-r_0^2)+\frac{3\beta}{8r_0^2}\sum_{i=1}^{4}\sum_{j=1}^{4}\left[\mathbf{r}_i\cdot\mathbf{r}_j+\frac{r_0^2}{3}\right]^2, \tag{2.1}$$

where α is a bond-stretching parameter and β a bond-bending parameter, r_i is along the bond between an atom and its neighbors. Variables with subscript zero denote ideal crystalline values. A shortcoming of this formula is that its anharmonicity overestimates the energy of a bond which is stretched above the harmonic limit. Keating has proposed a more complicated formula which better describes crystal anharmonicity:

$$E_K^{\mathrm{anh}}=E_K^H+\frac{\gamma'\sqrt{3}}{4r_0^3}\sum_{i=1}^{4}(\mathbf{r}_i\cdot\mathbf{r}_i+r_0^2)^3+\frac{\delta'\sqrt{3}}{2r_0^3}\sum_{i=1}^{4}\sum_{j<1}^{4}\left[\mathbf{r}_i\cdot\mathbf{r}_j+\frac{r_0^2}{3}\right]^3+\frac{\varepsilon'\sqrt{3}}{4r_0^3}\sum_{i=1}^{4}\sum_{j<1}^{4}\left[\mathbf{r}_i\cdot\mathbf{r}_j+\frac{r_0^3}{3}\right]^2(\mathbf{r}_i\cdot\mathbf{r}_i+\mathbf{r}_j\cdot\mathbf{r}_j-2r_0^2)\,. \tag{2.2}$$

In some cases this formula can cause an infinite expansion in the relaxation process. We therefore adopted the formula suggested by Koizumi and Ninomiya[23] in their treatment of amorphous Ge:

$$E_K^{\text{anh}}=\frac{3\alpha}{16r_0^2}\sum_{i=1}^{4}(\mathbf{r}_i\cdot\mathbf{r}_i-r_0^2)^2\exp\left[\frac{4\sqrt{3}\gamma'}{3\alpha r_0}(\mathbf{r}_i\cdot\mathbf{r}_i-r_0^2)\right]+\frac{3\beta}{8r_0^2}\sum_{i=1}^{4}\sum_{j=1}^{4}\left[\mathbf{r}_i\cdot\mathbf{r}_j+\frac{r_0^2}{3}\right]^2\exp\left[\frac{2\varepsilon'\sqrt{3}}{3\beta r_0}(\mathbf{r}_i\cdot\mathbf{r}_i+\mathbf{r}_j\cdot\mathbf{r}_j-2r_0^2)\right]+\frac{\delta'\sqrt{3}}{2r_0^3}\sum_{i=1}^{4}\sum_{j=1}^{4}\left[\mathbf{r}_i\cdot\mathbf{r}_j+\frac{r_0^2}{3}\right]^3 . \tag{2.3}$$

Expanded for small $|r_i-r_0|$ this is the same as (2.2).

The procedure for generating the geometry of the periodic repeated supercell is as follows. The first step is to generate two layers of the lattice pattern for the ideal germanium crystal perpendicular to the dislocation direction $[1\bar{1}0]$ and then shift part of the pattern along the direction $[11\bar{2}]$ by a Burgers vector $\frac{1}{6}a(1,1,-2)$, where a is the lattice constant for Ge. By the isotropic linear elasticity theory[8] the resulting patterns adjusted and then by using formula (2.3) the atomic positions around the core of the dislocation (about 90–100 atoms) are determined by minimization of the total energy of the valence potential using a optimization algorithm until the total-energy converges. The dangling-bond atoms at the core of the dislocation were treated in the virtual neighbor approach.[10] The atomic positions for the here applied supercell of 256 atoms have been taken from Teichler.[24]

The supercell has a center of symmetry to include two 90° partial dislocations with opposite Burgers vectors. The periodicity of the supercell lattice is taken into account by imposing suitable boundary conditions during the relaxation of the atom row positions within one supercell. A strip of intrinsic stacking faults lies in between the two 90° partial dislocations which are apart from each other by a distance of about 28 Å. The distance is big enough to decouple the interaction between the two partial dislocations. The supercell contains 256 atoms and the interactions of the dislocations in neighboring supercells are sufficiently small. The sufficiently large supercell contains no unphysical bonds since by St. Venant's principle[25] the strain is zero at the supercell boundaries.

The translational vectors for the supercell are

$$\begin{aligned}\mathbf{t}_1&=(55.4\text{ Å})\mathbf{i}\ ,\\ \mathbf{t}_2&=(9.2\text{ Å})\mathbf{i}+(26.1\text{ Å})\mathbf{j}\ ,\\ \mathbf{t}_3&=(4.0\text{ Å})\mathbf{k}\ ,\end{aligned} \tag{2.4}$$

where $\mathbf{i}$, $\mathbf{j}$, $\mathbf{k}$ are unit vectors along x, y, and z directions.

Figure 1 shows the perspective view of the unreconctructed 90° glide partial dislocation for germanium. The dislocation line runs in the $[1\bar{1}0]$ direction. We can see the dangling bonds at the core for the dislocation. The atomic arrangement of our supercell viewed along the dislocation line, is shown in Fig. 2. The big dots are in the upper plane and the small dots are in the lower plane; the distance between the two planes is 2.0 Å.

B. Localized pseudopotential and orbital functions

The electrons in the supercell are described by the LCAO scheme. Similar to Louie,[20] we use Gaussian-type pseudopotential and atom-centered Gaussians as the localized orbitals. The advantage of employing Gaussian potential and orbitals is that the evaluation of all matrix elements in real space is analytically tractable.

The crystalline potential for germanium is taken to be the sum of individual pseudopotentials of the form

$$V(r)=\sum_{i=1}^{3}a_i e^{-b_i r^2}\ , \tag{2.5}$$

where the parameters a and b are determined from previous pseudopotentials which are known to yield good results both in bulk and surface calculations. Especially in the surface calculation this potential yields a result which is similar to the result obtained from a full self-consistent calculation. Ten Gaussian functions are used for each atom: two s-like Gaussian orbitals

$$e^{-\alpha r^2},\quad r^2e^{-\alpha r^2}\ , \tag{2.6}$$

three p-like Gaussian orbitals

$$xe^{-\alpha r^2},\quad ye^{-\alpha r^2},\quad ze^{-\alpha r^2}\ , \tag{2.7}$$

and five d-like Gaussian orbitals

$$\begin{aligned}&xye^{-\alpha r^2},\quad zxe^{-\alpha r^2},\quad yze^{-\alpha r^2}\ ,\\ &(y^2-z^2)e^{-\alpha r^2},\quad [(x^2-y^2-z^2)/\sqrt{3}]e^{-\alpha r^2}\ .\end{aligned} \tag{2.8}$$

Table I provides a list of the parameters used in this study.

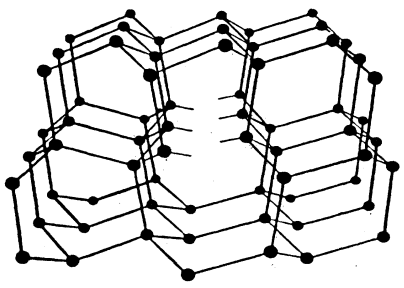

FIG. 1. Perspective view of the unreconstructed 90° glide partial dislocation. The dislocation line runs in the $\langle 1\bar{1}0\rangle$ direction.

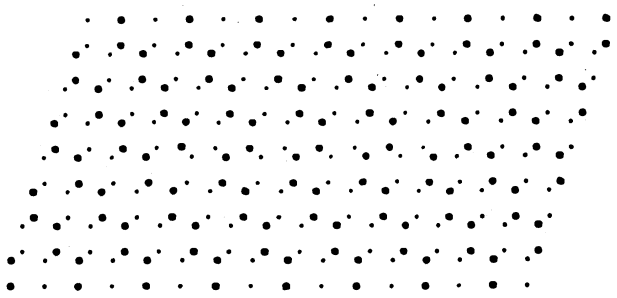

FIG. 2. The atomic arrangement of the supercell containing two 90° partial dislocations with opposite Burgers vectors, viewed along the dislocation direction. The big dots stand for the lattice points in the upper plane and the small dots for the ones in the lower plane.

All matrix elements for the Hamiltonian and overlap are evaluated with the interactions extending to the fourth nearest neighbors.

C. The translational symmetry

Because the atomic pattern for lattices with dislocation is periodic along the dislocation line, the Bloch wave number parallel to the dislocation line is conserved. The position vector for any atomic row can be expressed as

TABLE I. Potential parameters (the a's are in Ry and the b's in reciprocal Bohr radius squared) and orbital decay constants (in reciprocal Bohr radius squared).

α	a_1	b_1	a_2	b_2	a_3	b_3
0.17	15.97	0.57	−12.78	0.39	−2.68	0.81

$$\mathbf{R}_p^n=\mathbf{R}^n+(R_\parallel^n+pb)\mathbf{k}\ , \tag{2.9}$$

where R^n and $R_\parallel^n$ respectively, are the coordinates in the (x,y) plane and z direction and $\mathbf{k}$ is the unit vector in the z direction. We assume that the dislocation line is along this direction, p is an integer, and b denotes the translational vector in the z direction $b=a/\sqrt{2}$ (a is the lattice constant). The Bloch sum along the dislocation direction can be written as

$$\psi_k^{j,n}(\mathbf{r})=N^{-1/2}\sum_p \exp[ik(R_\parallel^n+pb)]\mu_j(\mathbf{r}-\mathbf{R}_p^n)\ , \tag{2.10}$$

where μ_j is the Gaussian orbital with symmetry j and k is the wave vector along the z direction $-\pi/b\le k\le\pi/b$.

The elements of the overlap matrices between the Bloch sums for the atomic rows can be written as

$$\begin{aligned}S_{i,j}^{m,n}(k)&=\langle i,m,k|j,n,k\rangle\ ,\\&=N^{-1}\sum_{p,q}\exp[-ik(R_\parallel^m+pb)]\exp[ik(R_\parallel^n+qb)]\langle i,m|j,n\rangle\ ,\\&=\exp[ik(R_\parallel^n-R_\parallel^m)]\sum_l \exp(iklb)\langle i,m|j,n\rangle\ ,\end{aligned} \tag{2.11}$$

where $l=q-p$ and

$$\langle i,m|j,n\rangle=\int dr^3\mu_i^*(r-R_p^m)\mu_j(r-R_q^n)\ . \tag{2.12}$$

The elements of the Hamiltonian matrices between the Bloch sums of the atomic rows are

$$\begin{aligned}H_{i,j}^{m,n}(k)&=\langle i,m,k|H|j,n,k\rangle\ ,\\&=N^{-1}\sum_{p,q}\exp[-ik(R_\parallel^m+pb)]\exp[ik(R_\parallel^n+qb)]\langle i,m|H|j,n\rangle\ ,\\&=\exp[ik(R_\parallel^n-R_\parallel^m)]\sum_l\exp(iklb)\langle i,m|H|j,n\rangle\ ,\end{aligned} \tag{2.13}$$

where $l=q-p$ and

$$\langle i,m|H|j,n\rangle=\int dr^3\mu_i^*(r-R_p^m)H\mu_j(r-R_q^n)\ . \tag{2.14}$$

In bulk the overlap matrices (2.12) and Hamiltonian matrices (2.14) are not negligible up to four nearest neighbors. In perfect crystal every atom has 35 neighboring atoms up to four nearest neighbors including itself and in our supercell every atom interacts with 17 atoms. In the case with dislocation as in the case of perfect crystals, every atomic row interacts with 17 neighboring rows including the row itself. The translational symmetry in the plane perpendicular to the dislocation line has been taken into account in the following way: the atomic rows near the boundaries of the supercell interact with the atomic rows outside the supercell. These interactions have been replaced by the interactions between the atomic rows and the translational counterparts of the atomic rows outside the supercell with the same matrix elements. The recursion procedure just as a propagation of "recursion wave:" the wave starts from the atomic row at the core of the dislocation propagates radially in the plane perpendicular to the dislocation line. When the wave hits the boundaries of the supercell it enters into the supercell again from the opposite side of the boundaries, as if the wave propagates in the plane with the periodicity of the supercell, but we can keep the calculation inside the supercell.

D. Recursion scheme

The Bloch sum (2.10) for the nonzero k in the one-dimensional Brillouin zone is complex. Hence the overlap matrix elements (2.11) and Hamiltonian matrix elements (2.13) for nonzero k along the dislocation line are also complex. For the convenience of the computation we should change the complex matrices into real matrices. This was achieved by a unitary transformation U:

$$\underline{U}=\frac{1}{\sqrt{2}}\begin{bmatrix}1 & 1\\ -i & i\end{bmatrix}. \tag{2.15}$$

Using the fact that the elements of $H(k)$ and $S(k)$ are complex conjugate to those of $H(-k)$ and $S(-k)$ we can combine the matrices for k and $-k$ by the transformation U. Owing to the time-reversal symmetry, the DOS for k and $-k$ are identical and the unitary transformation cannot change the DOS:

$$H'=U^{\dagger}HU=\tfrac{1}{2}\begin{bmatrix}H(k)+H(-k) & iH(k)-iH(-k)\\ -iH(k)+iH(-k) & H(k)+H(-k)\end{bmatrix}, \tag{2.16}$$

$$S'=U^{\dagger}SU=\tfrac{1}{2}\begin{bmatrix}S(k)+S(-k) & iS(k)-iS(-k)\\ -iS(k)+iS(-k) & S(k)+S(-k)\end{bmatrix}. \tag{2.17}$$

For every atomic row we have ten Bloch sums with different symmetry, in the supercell we have 256 atoms. After the U transformation, the overlap and Hamiltonian matrix will be of size 5120×5120.

The bound electron states of dislocation around the band gap are extracted using the Lanczos recursion approach for nonorthogonal basis functions[26] which is a slight generalization of the usual Haydock-Heine-Kelly[27] scheme.

The starting function can be expressed in the representation of the nonorthogonal basis $|\alpha\rangle$ as

$$|\psi_0\rangle=\sum_{\alpha}|\alpha\rangle u_0^{\alpha}, \tag{2.18}$$

where $|\alpha\rangle$ denotes the complex Bloch sum (2.10) and u_0^{α} is the weight of the starting function in the basis $|\alpha\rangle$. By the transformation (2.15) we can change every basis into real function and hence $|\psi_0\rangle$ become a real function. We denote with u_0 the column vector of the changed real starting function.

By using a symmetric three-term recurrence relation

$$b_{n+1}S'\mathbf{u}_{n+1}=H'\mathbf{u}_n-a_nS'\mathbf{u}_n-b_nS'\mathbf{u}_{n-1} \tag{2.19}$$

and the S orthonormality relation for the real set of orbitals $\{\mathbf{u}_0,\mathbf{u}_1,\dots\}$

$$\mathbf{u}_mS'\mathbf{u}_n=\delta_{m,n} \tag{2.20}$$

we can calculate the recursion coefficients

$$\begin{aligned}b_0&=\mathbf{u}_0^{\dagger}S'\mathbf{u}_0=1,\\ a_0&=\mathbf{u}_0^{\dagger}H'\mathbf{u}_0,\\ b_1&=[(\mathbf{u}_0^{\dagger}H'-a_0\mathbf{u}_0^{\dagger}S')(S')^{-1}(H'\mathbf{u}_0-a_0S'\mathbf{u}_0)]^{1/2},\\ \mathbf{u}_1&=(S')^{-1}(H'\mathbf{u}_0-a_0S'\mathbf{u}_0)/b_1.\end{aligned} \tag{2.21}$$

For the next step we have

$$\begin{aligned}a_1&=\mathbf{u}_1^{\dagger}H'\mathbf{u}_1,\\ b_2&=[(\mathbf{u}_1^{\dagger}H'-a_1\mathbf{u}_1^{\dagger}S'-b_1u_0^{\dagger}S')(S')^{-1}\\ &\quad\times(H'\mathbf{u}_1-a_1S'\mathbf{u}_1-b_1S'\mathbf{u}_0)]^{1/2},\\ u_2&=(S')^{-1}(H'\mathbf{u}_1-a_1S'\mathbf{u}_1-b_1S'\mathbf{u}_0)/b_{2a},\end{aligned} \tag{2.22}$$

and proceeding further we can transform the Hamiltonian matrix into a tridiagonal matrix. The local Green's function corresponding to $\mathbf{u}_0$ can be expressed as a continued fraction,

$$G_0(E)=\cfrac{1}{E-a_0-\cfrac{b_1^2}{E-a_1-\cfrac{b_2^2}{E-a_2-\cfrac{b_3^2}{E-a_3-\ddots}}}} \tag{2.23}$$

and the local DOS is

$$n_0(E)=-\pi^{-1}\mathrm{Im}G_0(E+i\eta)|_{\eta\to0}. \tag{2.24}$$

The starting function were constructed from the Bloch sum of atomic orbitals with symmetry ν and wave vector $\mathbf{k}$ along the rows of dangling-bond atoms in the dislocation cores. Starting functions with symmetries s, p, and sp^3 have been applied, however, it was found that the energy positions of the bound states are independent of the starting function character.

The unitary transformed overlap matrix S' is a real 5120×5120 large sparse matrix. In the recursion procedure we need calculate the quantity $(S')^{-1}\mathbf{c}$, where $\mathbf{c}$ is a real column vector with 5120 components. We cannot invert the matrix in the usual way, however we calculate the quantity $(S')^{-1}\mathbf{c}$ by solving the equation $S'\mathbf{x}=\mathbf{c}$. In order to minimize the storage requirement a refined quotient tree ordering algorithm[28] was employed. By using this algorithm at every step of the recursion procedure when column vector $\mathbf{c}$ has changed we need not repeat the whole procedure, hence the algorithm can also save very much computer time.

III. RESULTS AND DISCUSSION

The calculated dispersion curve of the band structure along the wave vector $\mathbf{k}$ parallel to the dislocation line for Ge with 90° partial dislocations was shown in Fig. 3. In the one-dimensional Brillouin zone we have calculated

$k=\pi n/6b$ for $n=0,1,\ldots,6$. Where $b=a/\sqrt{2}$, $a=5.658$ Å is the lattice constant of germanium. The deep levels in the gap and the resonant states in the band continuum were extracted using the Lanczos algorithm and a continued-fraction representation of the local density of states. Two defect bands were obtained for the 90° partial dislocation in germanium, and represented in Fig. 3 by dashed lines. In the center of the one-dimensional Brillouin zone the two bands are widely split and are joined together at the border of the Brillouin zone. The upper band is a resonant state near the center of the zone and becomes a bound state at the border of the zone. The lower band is a bound state over the whole zone.

Figures 4 and 5 illustrate the local density of states for 90° partial dislocation in germanium with the wave vector equal to $\pi/(2b)$ and π/b, respectively. The starting orbital is a sp^3 hybrid function at the dangling bonds of the dislocation core. We have pointed out that the position of the defect bands are independent of the symmetric characters of the starting orbitals. In Figs. 4 and 5 the local density of states are scaled with the same arbitrary unit.

In the region of k space near the center of the Brillouin zone the dislocation states interact strongly with the bulk-band states. At this points in k space the dislocation-state wave functions are, therefore, not strongly localized in the core region. Thus the peaks of the local density of states for the dislocation states are not very sharp. In the region of k space near the border of the Brillouin zone where the energies of the dislocation states are well outside the bulk projected band structure and are, consequently highly localized at the dislocation core. The peaks of the calculated density of states for the dislocation states are very sharp.

Experimentally in germanium[29,30] a partially filled band is found near the valence edge with the Fermi level, E_F, at $E_V+0.09$ eV. Cavallini *et al.*[31] find that this band drops as the deformation temperature increases. del Penino and Mantovani[32] show that the width of the lower band is about 0.18 eV in rough agreement with Schaumburg and Willmann.[33] Some other experiments show that there are two bands associated with the dislocations:[34–37] one close to the valence edge and the other in the upper half of the gap. Ossipyan[38] indicated that the lower band is a donor band and lies at 0.07 eV above the top of the valence band. The upper band is an acceptor band and lies at 0.5 eV beneath the bottom of the conduction band.

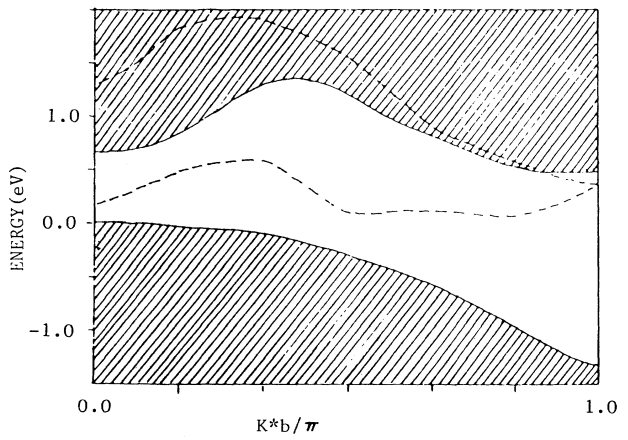

FIG. 3. The deep level structure of the unreconstructed 90° partial dislocations as a function of the k parallel to the dislocation line. The shadowed area represents the projections of the valence and the conduction bands. The dashed lines are the calculated bound (or resonant) electron states at the dangling bonds of the dislocation core.

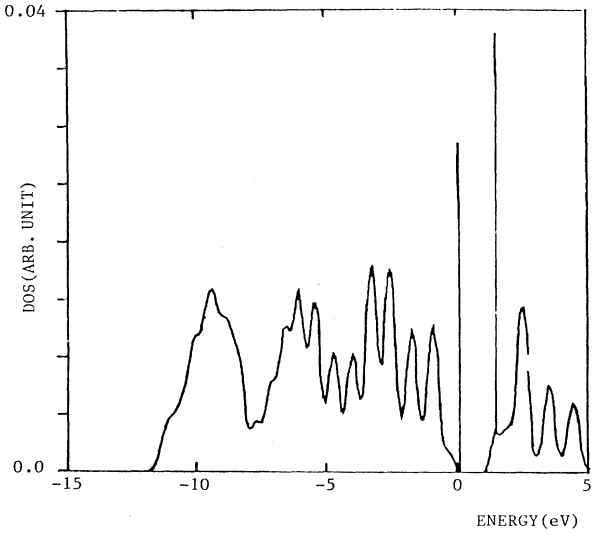

FIG. 4. The local density of the states with an sp^3 hybrid starting orbital at the dangling bonds of the dislocation core. The wave vector **k** is parallel to the dislocation line and is equal to $\pi/(2b)$.

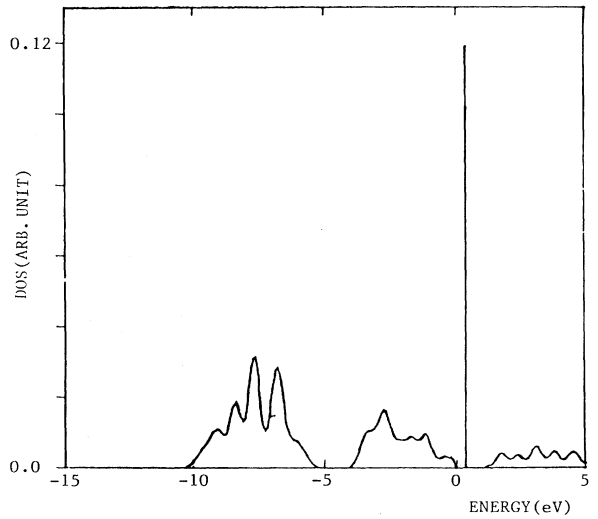

FIG. 5. The local density of the states with an sp^3 hybrid starting orbital at the dangling bonds of the dislocation core. The wave vector **k** is at the border of the one-dimensional Brillouin zone and is equal to π/b.

The Mott-Hubbard gap between the donor and acceptor dislocation bands is 0.18 eV.

It has been shown from the experiments on dislocations in real crystals that the length of the regular sections of the dislocation line is rather small (some tens or hundreds of interatomic distances). The regular sections in the dislocations alternate with local defects, such as jogs, points of intersection with other dislocations, split sections, etc. In addition some other defects may appear as impurity atoms, for example, oxygen, located near the core. That is the reason for which experiments have so far not succeeded in uniquely ascribing the observed levels to the different partials and to clearly decide whether the levels are associated with the ideal, straight partials or are due to special points on the dislocation cores.

There are not as many theoretical calculations for germanium[39,40] as for silicon. Veth and Teichler[40] have performed calculations for both unreconstructed and reconstructed 90° partial dislocations in germanium. Their calculations are based on a semiempirical one-electron tight-binding scheme with exponential scaling of the matrix elements under deformation. For unreconstructed 90° partial dislocations in germanium they found two defect bands in the lower half of the one-dimensional Brillouin zone. The two bands of bound states meet at the border of the zone. In the case of the reconstructed 90° partial dislocations in germanium these two bands are widely split and almost completely disappear in the band continuum.

Present calculations are based on more elaborate local-basis treatments, especially the interactions with *d* orbitals which for the first time have been taken accurately into account. The interactions with *d* orbitals are very sensitive to the changes of the relative positions of atoms. In the case of dislocations almost every atom is shifted from its positions in a perfect crystal.

We already pointed out that the low-symmetric reconstructed cores of partial dislocations without dangling bonds are energically more probable than the high-symmetric unreconstructed partial dislocations with dangling bonds in the core. The comparison of the present calculation with the results of experiments indicate that it is unlikely that the unreconstructed core geometry is the true geometry. Thus it would be significant to see how the two defect bands for unreconstructed 90° partial dislocations will shift when a calculation on reconstructed 90° partials is performed.

ACKNOWLEDGMENTS

I would like to express my sincere gratitude to Professor H. Teichler at the Institut für Metallphysik der Universität Göttingen for fruitful collaboration. Part of the computations was carried out at Gesellschaft für Wissenschaftliche Datenverarbeitung Göttingen (GWDG) of Göttingen University. I would also express my thanks to Professor Åke Björck at Linköping University for his helpful computational suggestions. Financial support from the Swedish Natural Science Research Council and Sonderforschungsbereich 126, Göttingen, Federal Republic of Germany, are gratefully acknowledged.

*Present address: Semiconductor Institute, Academia Sinica, P.O. Box 912, Beijing, People's Republic of China.

[1]R. Jones, in *Microscopy of Semiconducting Materials,* IOP Conf. Ser. No. 67 (IOP, London, 1981).
[2]S. Marklund, J. Phys. (Paris) Colloq. **44**, C4-25 (1983).
[3]H. Teichler and H. Veth, J. Phys. (Paris) Colloq. **44**, C4-93, (1983).
[4]R. Labusch and W. Schröter, *Dislocations in Solids,* edited by F.R.N. Nabaro (North-Holland, Amsterdam, 1980), Vol. 5, p. 127.
[5]I. L. F. Ray, and D. J. H. Cockayne, Proc. R. Soc. London, Ser. A **325**, 543 (1971).
[6]F. Häussermann and H. Schaumburg, Philos. Mag. **27**, 745 (1973).
[7]A. Gomes, D. J. H. Cockayne, P. B. Hirsch, and V. Vitek, Philos. Mag. **31**, 105 (1975).
[8]J. P. Hirth and J. Lothe, *Theory of Dislocations* (McGraw-Hill, New York, 1968); IOP Conf. Proc. No. 60 (IOP, London), p. 45.
[9]K. Wessel and H. Alexander, Philos. Mag. **35**, 1523 (1977).
[10]S. Marklund, Phys. Status Solidi B **92**, 83 (1979); *ibid.* B **100**, 77 (1980).
[11]J. R. Chelikowsky and J. C. H. Spence, Phys. Rev. B **30**, 694 (1984).
[12]A. Persson, Phys. Status Solidi B **113**, 253 (1982).
[13]R. Jones, J. Phys. (Paris) Colloq. **40**, C 60-33 (1979).
[14]R. Jones and S. Marklund, Phys. Status Solidi B **101**, 585 (1980).
[15]R. Haydock in *Solid State Physics,* edited by H. Ehrenreich, F. Seitz, and D. Turnbull (Academic, New York, 1980), Vol. 35, p. 215.
[16]J. C. Slater and G. F. Koster, Phys. Rev. **94**, 1498 (1954).
[17]K. C. Pandey and J. C. Phillips, Phys. Rev. B **13**, 750 (1976).
[18]J. E. Northrup, M. L. Cohen, J. R. Chelikowsky, J. Spence, and A. Olsen, Phys. Rev. B **24**, 4623 (1981).
[19]J. R. Chelikowsky, Phys. Rev. Lett. **49**, 1569 (1982).
[20]S. G. Louie, Phys. Rev. B **22**, 1933 (1980).
[21]Wang Yong-liang and H. Teichler (unpublished).
[22]P. N. Keating, Phys. Rev. **145**, 637 (1966); **149**, 674 (1966).
[23]H. Koizumi and T. Ninomiya, J. Phys. Soc. Jpn. **44**, 898 (1978).
[24]H. Teichler (private communication).
[25]*Handbook of Physics,* edited by E. U. Condon and H. Odishaw (McGraw-Hill, New York, 1958), pp. 3–64.
[26]Wang Yong-liang and U. Lindefelt, Phys. Rev. B **37**, 1320 (1988).
[27]R. Haydock, V. Heine and M. J. Kelly, J. Phys. (Paris) Colloq. **36**, C8-2591 (1975).
[28]J. A. George and J. W. H. Liu, *Algorithm for Matrix Partitioning and the Numerical Solution of Finite Element Systems* [SIAM J. Numer. Anal. **15**, 297 (1978)].
[29]W. Schröter and R. Labusch, Phys. Status Solidi, B **36**, 539 (1969).
[30]R. Labusch and W. Schettler, Phys. Status Solidi A **9**, 455

(1972).
[31]A. Cavallini, P. Gondi, and A. Castaldina, Phys. Status Solidi, A **43**, K205 (1977).
[32]U. del Penino and S. Mantovani, Phys. Status Solidi A **38**, 109 (1976).
[33]H. Schaumburg and F. Willman, Phys. Status Solidi A **34**, K173 (1976).
[34]H. R. Weber, Phys. Status Solidi A **25**, 445 (1974).
[35]W. Barth and W. Guth, Phys. Status Solidi B **38**, K141 (1970).
[36]W. Barth and K. Elsässer, Phys. Status Solidi B **48**, K147 (1971).
[37]M. Jastrzeksha and T. Figielski, Phys. Status Solidi B **32**, 791 (1969).
[38]Yu A. Ossipyan, J. Phys. (Paris) Colloq. **44**, C4-103 (1983).
[39]S. Marklund, Phys. Status Solidi B **85**, 673 (1978).
[40]H. Veth and H. Teichler, Philos. Mag. B **49**, 371 (1984).